INSTITUTE OF MATHEMATICS

THE CZECH ACADEMY OF SCIENCES

A conservative scheme for the Fokker-Planck equation with applications to viscoelastic polymeric fluids

Hana Mizerová
Bangwei She

Preprint No. 34-2018

PRAHA 2018

A conservative scheme for the Fokker-Planck equation with applications to viscoelastic polymeric fluids

Hana Mizerová [a,b] Bangwei She [b,*]

[a] Department of Mathematical Analysis and Numerical Mathematics
Faculty of Mathematics, Physics and Informatics of the Comenius University
Mlynská dolina, 842 48 Bratislava, Slovakia

[b] Institute of Mathematics, the Czech Academy of Sciences
Žitná 25, CZ-115 67 Praha 1, Czech Republic

Abstract

We propose a conservative scheme for a high-dimensional Fokker-Planck equation that arises in the dynamics of infinitely extensible polymer molecules. This leads to a challenging problem of unbounded domain. Our scheme combines the Lagrange-Galerkin method and the Hermite spectral method together with a space splitting approach. We prove that the scheme preserves the discrete mass. Combining it with a stabilized Lagrange-Galerkin method for the Navier-Stokes equations, we further propose a multiscale scheme for the simulation of some viscoelastic polymeric fluids. Several numerical experiments are presented to illustrate the performance of the schemes, and to confirm the conservation of mass at the discrete level.

Keywords: Lagrange-Galerkin method; Hermite spectral method; Navier-Stokes; Fokker-Planck; Kinetic dumbbell model; Viscoelastic fluids;

*Correspondence to she@math.cas.cz.

The research of H.M. leading to these results has received funding from the Czech Sciences Foundation (GAČR), Grant Agreement 18–05974S. The research of B.S. has been supported by the Czech Sciences Foundation (GAČR), Grant Agreement 16–03230S. The Institute of Mathematics of the Czech Academy of Sciences is supported by RVO:67985840.

1 Introduction

The Fokker-Planck equation was firstly used to describe the Brownian motion of particles. It arises in different fields of physics, biology, chemistry and mathematics such as plasma physics, astrophysics, laser arrays, electronic circuity, neurophysics, population dynamics, pattern formation and also marketing, cf. [12, 27]. We are interested in its application in polymeric fluids and particle beams, see, e.g., [2, 6, 9, 26].

In particular, we study the behaviour of infinitely extensible polymer molecules, not interacting with each other, that are suspended in a solvent. The distribution of the polymers is described by a high-dimensional nonlinear Fokker-Planck equation for the probability density function that is defined both in the bounded physical space $\Omega \subset \mathbb{R}^d$ and in the infinite configuration space $\mathfrak{D} := \mathbb{R}^d$, $d = 2, 3$. More precisely, the probability density function $\psi = \psi(t, \mathbf{x}, \mathbf{R}) : [0, T] \times \Omega \times \mathfrak{D} \to \mathbb{R}$ satisfies

$$\frac{\partial \psi}{\partial t} + \mathbf{u} \cdot \nabla_x \psi - \varepsilon \Delta_x \psi = -\nabla_R \cdot \big(\nabla_x \mathbf{u} \cdot \mathbf{R}\psi\big) + \nabla_R \cdot \big(\xi \mathbf{R}\psi\big) + \chi \Delta_R \psi. \tag{1}$$

Here the constant $\varepsilon \geq 0$ stands for the centre-of-mass diffusion coefficient, the velocity of the solvent $\mathbf{u}$ and the real functions ξ, χ defined in $[0, T] \times \Omega$ are given. It is worth mentioning that the functions ξ, χ and the parameter ε are inversely proportional to the relaxation time (or Weissenberg number), which is a well-known concept in the rheology of polymeric fluids. We refer to [4, 13, 26] for more details. Note that

$$\int_{\mathfrak{D}} \psi(t, \mathbf{x}, \mathbf{R})\, d\mathbf{R} = 1, \quad \forall (t, \mathbf{x}) \in [0, T] \times \Omega. \tag{2}$$

The equation is equipped with the decay/boundary and initial conditions,

$$\psi|_{|\mathbf{R}| \to \infty} = 0, \quad \frac{\partial \psi}{\partial \mathbf{n}}|_{\partial\Omega} = \mathbf{0}, \tag{3}$$

$$\psi(0) = \psi^0, \tag{4}$$

where $\psi_0 : \Omega \times \mathfrak{D} \to \mathbb{R}$ is a suitable initial value. Note that throughout the paper we might omit the dependence of functions on the variables $t, \mathbf{x}, \mathbf{R}$ when there is no confusion.

The numerical solution of the Fokker-Planck equation confined to a single (configuration) space, that is either finite or infinite, has been already widely studied, see, e.g., [11, 22, 30]. On the other hand, in [7, 15, 16, 18, 32] the authors proposed numerical schemes for equation (1) considered both in the physical and the configuration space, however, restricted to the finite spaces only. To the best of our knowledge there is no numerical scheme for the high-dimensional Fokker-Planck equation in the case of infinite configuration space and finite physical space. The main aim of this paper is to propose such a scheme that is based on the Lagrange-Galerkin method and the Hermite spectral method. Another goal is to combine

this scheme with a stabilized Lagrange-Galerkin method for the Navier-Stokes equations in order to simulate some viscoelastic polymeric fluid flows.

The rest of the paper is organized as follows. In Section 2 we describe a space splitting technique and numerical methods. In the next section we propose the numerical scheme and prove that it is, at the discrete level, mass preserving with respect to the probability density function ψ. Moreover, we validate the scheme by some numerical examples. In Section 4 we extend it to a multiscale solver for the Navier-Stokes-Fokker-Planck system.

2 Numerical method

Since the Fokker-Planck equation (1) involves both the configuration space ($\mathbf{R} \in \mathfrak{D} = \mathbb{R}^d$) and the physical space ($\mathbf{x} \in \Omega \subset \mathbb{R}^d$), it is convenient to decompose it into two parts accordingly. For the approximation of the Fokker-Planck equation in the configuration space we adopt the Hermite spectral method, which is naturally designed for an unbounded domain, cf. [11]. To solve the equation in the physical space we use the Lagrange-Galerkin method.

Firstly, we discretize the time interval $[0, T]$ into N_T equidistant parts, and denote by $t^n = n\Delta t$ for $n \in \{0, 1, \cdots, N_T\}$ the current time step, and by $\Delta t = \frac{T}{N_T}$ the fixed time increment.

2.1 Space splitting

Following the idea of Lozinski and Chauvière [7] or Knezevic and Süli [15] we consider the space splitting method defined below.

Definition 1. (Space splitting)
Firstly, we fix a point in the physical space $\mathbf{x} \in \Omega$ and solve the first part of (1) in the configuration space $\mathfrak{D}$,

$$\frac{\psi^* - \psi^n}{\Delta t} = \nabla_R \cdot \left((-\nabla_x \mathbf{u}^n \cdot \mathbf{R} + \xi \mathbf{R}) \psi^* \right) + \chi \Delta_R \psi^*, \quad \mathbf{R} \in \mathfrak{D}. \tag{5}$$

In the second step we fix the point in the configuration space $\mathbf{R} \in \mathfrak{D}$ and solve the rest of (1) in the physical space Ω,

$$\frac{\psi^{n+1} - \psi^*}{\Delta t} - \mathbf{u}^n \cdot \nabla_x \psi^* - \varepsilon \Delta_x \psi^{n+1} = 0, \quad \mathbf{x} \in \Omega. \tag{6}$$

2.2 Lagrange-Galerkin method

In what follows we briefly explain the Lagrange-Galerkin method which was used in [24] for the Navier-Stokes equations. It employs the following first-order approximation of the material derivative $\mathrm{D}g/\mathrm{D}t$ of a function $g : [0, T] \times \Omega \to \mathbb{R}$,

$$\frac{\mathrm{D}g}{\mathrm{D}t}(t^n, \mathbf{x}) := \left(\frac{\partial g}{\partial t} + (\mathbf{u} \cdot \nabla_x) g \right)(t^n, \mathbf{x}) = \frac{g^n(\mathbf{x}) - (g^{n-1} \circ X_1)(\mathbf{x})}{\Delta t} + O(\Delta t), \tag{7}$$

where $X_1 : \Omega \to \mathbb{R}^d$ is a mapping defined by $X_1(\mathbf{w}, \Delta t)(\mathbf{x}) := \mathbf{x} - \mathbf{w}(\mathbf{x})\Delta t$. Note that for $\mathbf{w} \in W_0^{1,\infty}(\Omega)^d$ and the time increment satisfying $\Delta t < 1/\|\mathbf{w}\|_{1,\infty}$, it holds that $X_1(\mathbf{w}, \Delta t)(\Omega) = \Omega$, see [24, 28, Proposition 1].

The symbol $\circ$ means the composition of functions, $(g^{n-1} \circ X_1)(\mathbf{x}) := g^{n-1}(X_1(\mathbf{x}))$ with $g^n(\mathbf{x}) := g(t^n, \mathbf{x})$. Approximation (7) following the trajectory of particles backward in time has appeared as a powerful tool for numerical solution of equations describing fluid motion, see, e.g., [10, 19–21, 28].

Let Ω be a polygonal domain, $\mathcal{T}_h$ a triangulation of $\bar{\Omega} := \bigcup_{K \in \mathcal{T}_h} K$, h_K the diameter of element $K \in \mathcal{T}_h$, $h := \max_{K \in \mathcal{T}_h} h_K$ the maximum element size, and $\mathcal{V}_h$ the set of all vertices $\mathbf{x}_i$ in $\mathcal{T}_h$. We consider a regular family of subdivisions $\{\mathcal{T}_h\}_{h \downarrow 0}$ satisfying the inverse assumption [8]. We consider a conforming finite element approximation of the probability density function satisfying the part of the Fokker-Planck equation (6) corresponding to the physical space. To this end we define the following finite element spaces

$$X_h^m := \{\mathbf{v}_h \in C^0(\bar{\Omega})^m; \mathbf{v}_h|_K \in \mathcal{P}^1(K)^m, \forall K \in \mathcal{T}_h\}, \ m \geq 1, \quad W_h := X_h^1,$$

where $\mathcal{P}^1(K)$ is the polynomial space of linear functions on element K. For more details on the Lagrange-Galerkin method we refer the reader to [23–25, 33] and the references therein.

2.3 Hermite spectral method for an unbounded domain

In order to deal with the problem of the infinite configuration space we consider a spectral method based on the weighted Hermite polynomials, that have already been used to derive numerical methods for problems on unbounded domains, see, for instance, [11, 31].

Before we derive the spectral method, let us introduce the definition and useful properties of the *Weighted Hermite polynomial [22]*. It is defined for $r \in \mathbb{R}$ as

$$\tilde{H}_m(r) := \frac{\omega_\alpha}{\sqrt{2^m m!}} H_m(\alpha r), \ \omega_\alpha(r) := e^{\alpha^2 r^2}, \ \alpha > 0, \ m \geq 0, \tag{8}$$

where the Hermite polynomial of degree m is given by

$$H_m(r) := (-1)^m e^{r^2} \partial_r^m (e^{-r^2}), \ r \in \mathbb{R}. \tag{9}$$

The weighted Hermite polynomials are orthogonal with respect to the weight ω_α,

$$\int_{\mathbb{R}} \tilde{H}_m(r) \tilde{H}_n(r) \omega_\alpha(r) = \frac{\sqrt{\pi}}{\alpha} \delta_{mn}, \tag{10}$$

δ_{mn} being the Kronecker delta. Moreover, they satisfy the following properties that shall be used for the derivation of the configuration space solver (16) below.

Namely,

$$\alpha r\tilde{H}_m(r) = \sqrt{\frac{m+1}{2}}\tilde{H}_{m+1}(r) + \sqrt{\frac{m}{2}}\tilde{H}_{m-1}(r), \tag{11a}$$

$$\frac{d}{dr}\tilde{H}_m(r) = -\alpha\sqrt{2(m+1)}\tilde{H}_{m+1}(r), \tag{11b}$$

$$r\frac{d}{dr}\tilde{H}_m(r) = -\sqrt{(m+1)(m+2)}\tilde{H}_{m+2}(r) - (m+1)\tilde{H}_m(r), \tag{11c}$$

$$\frac{d^2}{dr^2}\tilde{H}_m(r) = 2\alpha^2\sqrt{2(m+1)(m+2)}\tilde{H}_{m+2}(r). \tag{11d}$$

Another useful feature of this function is

$$\tilde{H}_m(r) \longrightarrow 0 \text{ as } r \longrightarrow \infty. \tag{12}$$

We refer the reader to, e.g., [11,30,34] and the references therein for the definition and an overview of the properties of the weighted Hermite polynomials.

We shall use the following quadrature rule for integrals in $\mathbb{R}$.

Theorem 2.1. [30, Theorem 7.3] (Hermite-Gauss quadrature)
Let $\{r_i\}_{i=0}^N$ be the zeros of $H_{N+1}(r)$, and $\{w_i\}_{i=0}^N$ be the weights given by

$$w_i := \frac{2^N\sqrt{\pi}N!}{(N+1)H_N^2(r_i)}, \quad 0 \le i \le N.$$

Then,

$$\int_{\mathbb{R}} p(r)\mathrm{e}^{-r^2}\,dr = \sum_{i=0}^{N} p(r_i)w_i, \quad p \in \mathcal{P}^{2N+1}(\mathbb{R}). \tag{13}$$

For the simplicity of notation and better readability let us fix the dimension to $d = 2$ hereafter. Note that the method can be analogously derived for $d = 3$. Let $\mathbf{R} := (r_1, r_2) \in \mathfrak{D} = \mathbb{R}^2$. We define a grid point $\mathbf{R}_{ij} := (r_{1,i}, r_{2,j})$ with $r_{1,i}$ and $r_{2,j}$ being the roots of the Hermite polynomial $H_{N+1}(r)$. Consequently, we can define the mesh $\mathfrak{D}_N$ as the set of $(N+1)\times(N+1)$ grid points $\mathbf{R}_{ij}$, i.e.,

$$\mathfrak{D}_N := \big\{\mathbf{R}_{ij} = (r_{1,i}, r_{2,j}),\, i,j = 0,1,\cdots,N;\, H_{N+1}(r_{1,i}) = H_{N+1}(r_{2,j}) = 0\big\}. \tag{14}$$

To solve the equation (5) we use the spectral method based on the weighted Hermite polynomials introduced above. To this end we define the spaces $P_N :=$ span $\{\tilde{H}_m(r)\}_{m=0}^N$, and $P_N^2 := P_N \otimes P_N$. We seek an approximate solution $\psi_{h,N} \in W_h \otimes P_N^2$ in the form

$$\psi_{h,N}^n(\mathbf{x},\mathbf{R}) = \sum_{i=0}^{N}\sum_{j=0}^{N} \phi_{ij}^n(\mathbf{x})\,\tilde{H}_i(r_1)\tilde{H}_j(r_2),\ \forall\, t^n,\ n = 0,\ldots,N_T. \tag{15}$$

Remark 1. *The property (12) together with the spectral decomposition (15) directly imply that the decay boundary condition $\psi|_{|\mathbf{R}|\to\infty} = 0$ is satisfied at the discrete level.*

3 Conservative scheme

In what follows we derive the numerical scheme for the Fokker-Planck equation (1).

Configuration space solver We insert (15) into equation (5), multiply it with the test function $\tilde{H}_z(r_1)\tilde{H}_k(r_2)\omega_\alpha(r_1)\omega_\alpha(r_2)$, and integrate over the configuration space $\mathfrak{D}$. After employing the orthogonality (10) and the properties (11) of the weighted Hermite polynomials we obtain the following *finite difference* scheme:

$$\frac{\phi^*_{zk} - \phi^{n-1}_{zk}}{\Delta t}(\mathbf{x}_i) = \mathbb{L}(\phi^*_{zk}(\mathbf{x}_i)), \quad \mathbf{x}_i \in \mathcal{V}_h, \quad z,k = 0,\dots,N, \tag{16}$$

where

$$\begin{aligned}\mathbb{L}(\phi_{zk}) := {} & \phi_{z-2,k}(2\alpha^2\chi - A_{11})\sqrt{z(z-1)} + \phi_{z-1,k-1}(-A_{12} - A_{21})\sqrt{zk} \\ & + \phi_{z-1,k+1}(-A_{12})\sqrt{z(k+1)} + \phi_{z,k-2}(2\alpha^2\chi - A_{22})\sqrt{k(k-1)} \\ & + \phi_{z,k}(-A_{11}z - A_{22}k) + \phi_{z+1,k-1}(-A_{12})\sqrt{(z+1)k},\end{aligned} \tag{17}$$

and $A_{ij} := -\partial_j u_i + \xi\delta_{ij}$. Note that $\phi_{z,k} \equiv 0$ if any of z,k is less than 0 or greater than N.

Physical space solver We insert (15) into (6), multiply it with the test function $\tilde{H}_z(r_1)\tilde{H}_k(r_2)\omega_\alpha(r_1)\omega_\alpha(r_2)\varphi_h$, and integrate over both the configuration space $\mathfrak{D}$ and the physical domain Ω. Consequently, using the Lagrange-Galerkin method introduced in Subsection 2.2 we derive an equation for the unknowns ϕ^n_{zk}. It reads

$$\left(\frac{\phi^n_{zk} - \phi^*_{zk} \circ X_1(\mathbf{u}^{n-1}, \Delta t)}{\Delta t}, \varphi_h\right) + \varepsilon(\nabla_x \phi^n_{zk}, \nabla_x \varphi_h) = 0, \quad z,k = 0,\dots,N. \tag{18}$$

Combining the above derived solvers (16) and (18) we propose the scheme.

Definition 2. (Scheme for the Fokker-Planck equation)
Let $\mathbf{u}$ *be sufficiently smooth such that* $X_1(\Omega) = \Omega$. *We seek* $\{\phi^n_{zk}\}_{n=1}^{N_T} \subset W_h$ *satisfying*

$$\frac{\phi^*_{zk}(\mathbf{x}_i) - \phi^{n-1}_{zk}(\mathbf{x}_i)}{\Delta t} = \mathbb{L}(\phi^*_{zk}(\mathbf{x}_i)) \quad \text{for } z,k = 0,\dots,N \text{ and a fixed } \mathbf{x}_i \in \mathcal{V}_h, \tag{19a}$$

$$\left(\frac{\phi^n_{zk} - \phi^*_{zk} \circ X_1(\mathbf{u}^{n-1}, \Delta t)}{\Delta t}, \varphi_h\right) + \varepsilon(\nabla_x \phi^n_{zk}, \nabla_x \varphi_h) = 0 \quad \text{in } \Omega \text{ for fixed } z,k, \tag{19b}$$

for any test function $\varphi_h \in W_h$. *Consequently, the approximate solution* $\{\psi^n_{h,N}\}_{n=1}^{N_T} \in W_h \times P_N^2$ *is computed from* $\phi_{zk}(\mathbf{x}_i)$ *by*

$$\psi^n_{h,N}(\mathbf{x}_i, \mathbf{R}_{lj}) = \sum_{z=0}^{N}\sum_{k=0}^{N} \phi^n_{zk}(\mathbf{x}_i)\, \tilde{H}_z(r_{1,l})\tilde{H}_k(r_{2,j}), \quad \text{for } \mathbf{x}_i \in \mathcal{V}_h \text{ and } \mathbf{R}_{lj} \in \mathfrak{D}_N.$$

The initial values $\phi_{zk}^0(\mathbf{x}_i)$ for all $\mathbf{x}_i \in \mathcal{V}_h$ are computed from $\psi^0(\mathbf{x}, \mathbf{R})$ through the spectral decomposition (15).

Remark 2. *The scheme (19) has no requirements on the time increment Δt. Indeed, the Lagrange-Galerkin method in (18) has no limitation on the time step due to the discretization of material derivative along the trajectory curve. The Hermite spectral method (16) neither needs a CFL condition as it is implicit.*

3.1 Conservation of mass

The Hermite spectral method allows us to show the discrete counterpart of the conservation of mass which is one of the important features of numerical schemes.

Theorem 3.1. (Discrete conservation of mass)
Let $\psi_{h,N} \in W_h \times P_N^2$ be the solution of the scheme (19). Let the initial probability density function be such that $\psi(0, \mathbf{x}, \mathbf{R}) = \psi^0(\mathbf{R})$.
Then, for any $n \in \{1, \dots, N_T\}$, it holds that

$$\int_{\mathfrak{D}} \psi_{h,N}^n(\mathbf{R})\, d\mathbf{R} = \int_{\mathfrak{D}} \psi_{h,N}^0(\mathbf{R})\, d\mathbf{R}.$$

The proof of Theorem 3.1 comes after two preliminary lemmas.

Lemma 3.2.
Let the assumptions of Theorem 3.1 be satisfied. Then, $\phi_{00}^n(\mathbf{x})$ is constant for all $\mathbf{x} \in \Omega$ and any time t^n, $n \in \{1, \dots, N_T\}$.

Proof. The proof is done by induction for n.

- By the assumption of the lemma the coefficients ϕ_{zk}^0 are independent of $\mathbf{x}$. In particular, ϕ_{00}^0 is constant in Ω.
- Assume $\phi_{00}^{n-1}(\mathbf{x}) = \phi_{00}^{n-1}$ is a constant function in Ω. Then equation (19a) with (17) directly yields $\phi_{00}^*(\mathbf{x}_i) = \phi_{00}^{n-1}(\mathbf{x}_i) = \phi_{00}^{n-1}$. By the Lax-Milgram theorem [17], equation (19b) has a unique solution ϕ_{zk}^n for any $z, k \in \{0, \dots, N\}$. We know that for $z = k = 0$ the constant ϕ_{00}^* is the solution, since $\phi_{00}^* \circ X_1^n = \phi_{00}^*$. Thus $\phi_{00}^n(\mathbf{x}) = \phi_{00}^* = \phi_{00}^{n-1}$. This concludes the proof.

□

We now recall another useful property of the weighted Hermite polynomials.

Lemma 3.3. [22, Lemma 4]
For the weighted Hermite polynomial $\tilde{H}_m(r)$ it holds that

$$\int_{\mathbb{R}} \tilde{H}_m(r)\, dr = 0, \text{ for any } m \geq 1.$$

Proof of Theorem 3.1. The conservation of mass at the discrete level is a direct consequence of Lemmas 3.2 and 3.3. Indeed, we have

$$\begin{aligned}\int_{\mathfrak{D}} \psi^n_{h,N}(\mathbf{R})\, d\mathbf{R} &= \int_{\mathfrak{D}} \sum_{z,k=0}^{N} \phi^n_{zk} \tilde{H}_z(r_1)\tilde{H}_k(r_2)\, d\mathbf{R} = \int_{\mathfrak{D}} \phi^n_{00}\tilde{H}_0(r_1)\tilde{H}_0(r_2)\, d\mathbf{R} \\ &= \int_{\mathfrak{D}} \phi^0_{00}\tilde{H}_0(r_1)\tilde{H}_0(r_2)\, d\mathbf{R} = \int_{\mathfrak{D}} \sum_{z,k=0}^{N} \phi^0_{zk} \tilde{H}_z(r_1)\tilde{H}_k(r_2)\, d\mathbf{R} \\ &= \int_{\mathfrak{D}} \psi^0_{h,N}(\mathbf{R})\, d\mathbf{R},\end{aligned}$$

which concludes the proof. □

3.2 Numerical experiments

We present three numerical experiments in order to demonstrate the performance of the proposed scheme, and to validate the conservation of mass as stated in Theorem 3.1. To this end we take the initial value independent of $\mathbf{x}$. More precisely, we set $\psi^0(\mathbf{x}, \mathbf{R}) = M(\mathbf{R})$, where the Maxwellian reads

$$M(\mathbf{R}) = \frac{1}{2\pi} \mathrm{e}^{-|\mathbf{R}|^2/2}. \tag{20}$$

Some discussions and suggestions on how to choose the weight α can be found in [11, 22]. We have set $\alpha = 0.5$ in all the tests. In Experiments 1 and 2 below we test two periodic flows in the physical domain $\Omega = [0, 1]^2$.

Experiment 1 We consider a *shear flow* with the velocity field $\mathbf{u} = (x_2, 0)^T$ and $\varepsilon = \xi = \chi = 1$. We set $\Delta t = 0.05$ and $N = 21$. Figure 1 shows the evolution of the probability density function towards the steady state.

Experiment 2 We set $\mathbf{u} = (x_2(1 - x_2), 0)^T$, $\xi = \chi = 1$, and $\varepsilon = 0.01$. The discretization parameters are chosen as $h = 1/64$, $\Delta t = 0.1$ and $N = 21$. Figure 2 shows the distribution of ψ in configuration space at different physical space points at time $t = 10$.

Experiment 3 To provide a quantitative study of the numerical accuracy we now consider an *extensional flow* with $\nabla_x \mathbf{u} = \mathrm{diag}\{\kappa, -\kappa\}$. In this case the exact steady-state solution of the Fokker-Planck equation is explicitly given by

$$\psi_{\mathrm{ref}}(\mathbf{R}) = cM\mathrm{e}^{\mathbf{R}^T \nabla_x \mathbf{u} \mathbf{R}},$$

where c is a normalization constant. We set $\xi = \chi = 1$ and the extension rate $\kappa = 0.5$. The numerical errors of the probability density function $e_\psi := \psi_{h,N} - \psi_{\mathrm{ref}}$ in $L^2(\mathfrak{D})$-norm and $L^\infty(\mathfrak{D})$-norm are listed in Table 1 with a fixed time step $\Delta t = 0.05$. We can clearly observe the experimental convergence of the solution

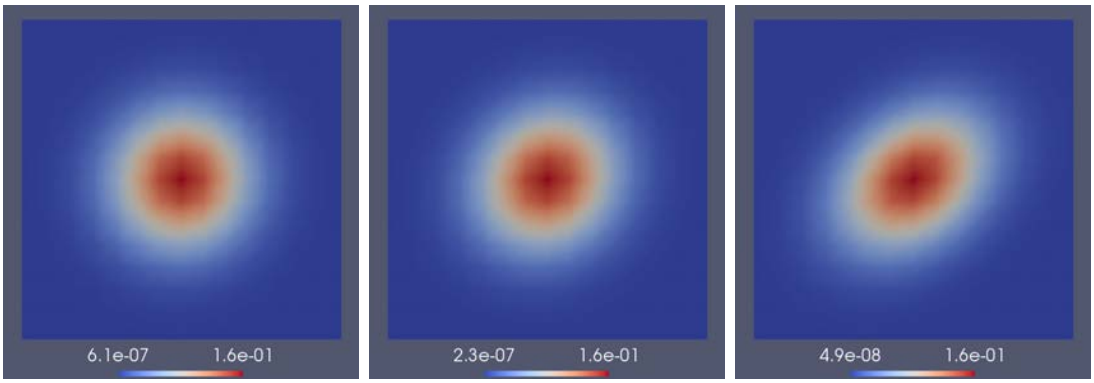

(a) t=0 (b) t=0.1 (c) t=0.5

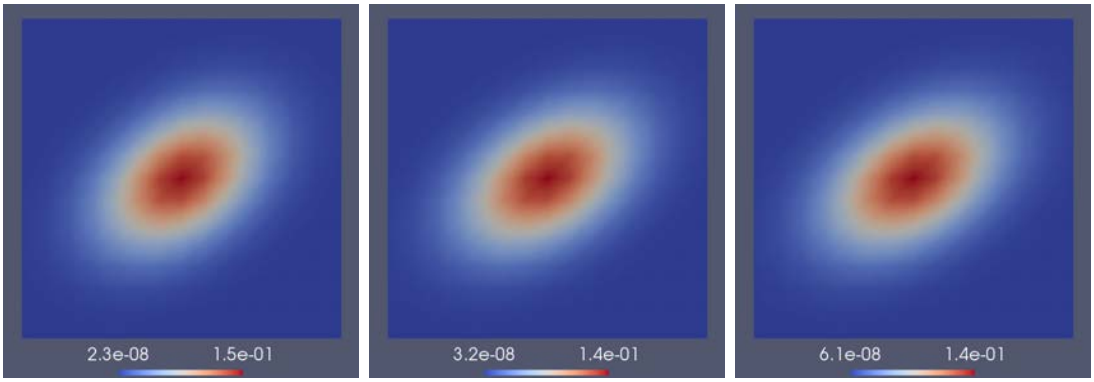

(d) t=1 (e) t=2 (f) t=10

Figure 1: Experiment 1: time evolution of ψ towards the steady state

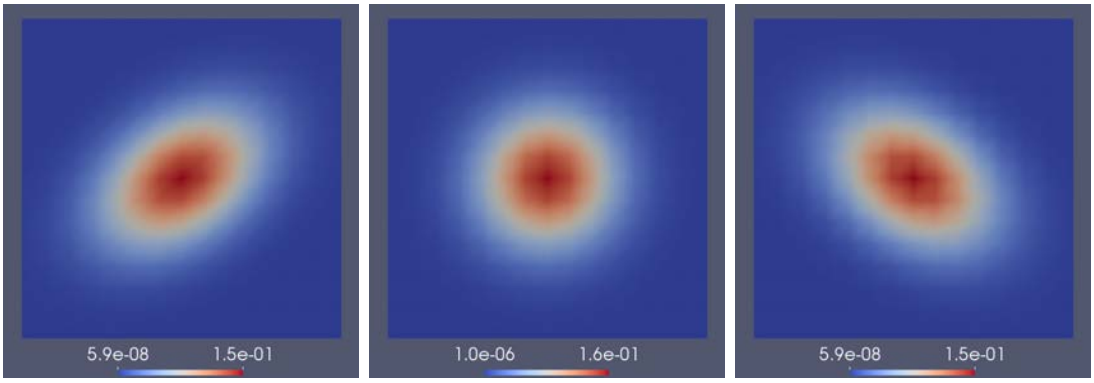

(a) $\mathbf{x} = (0.75, 0)$ (b) $\mathbf{x} = (0.75, 0.5)$ (c) $\mathbf{x} = (0.75, 1)$

Figure 2: Experiment 2: distribution of ψ in configuration space

with increasing polynomial degree N, and thus with an increasing number of the grid points $\mathbf{R}_{ij}$ in $\mathfrak{D}_N$. Figure 3 depicts the time evolution of ψ towards the steady state ψ_{ref} for $N = 40$.

Conservation of mass In Theorem 3.1 we have shown not only that the scheme is mass conservative, but also that the discrete mass only depends on the choice

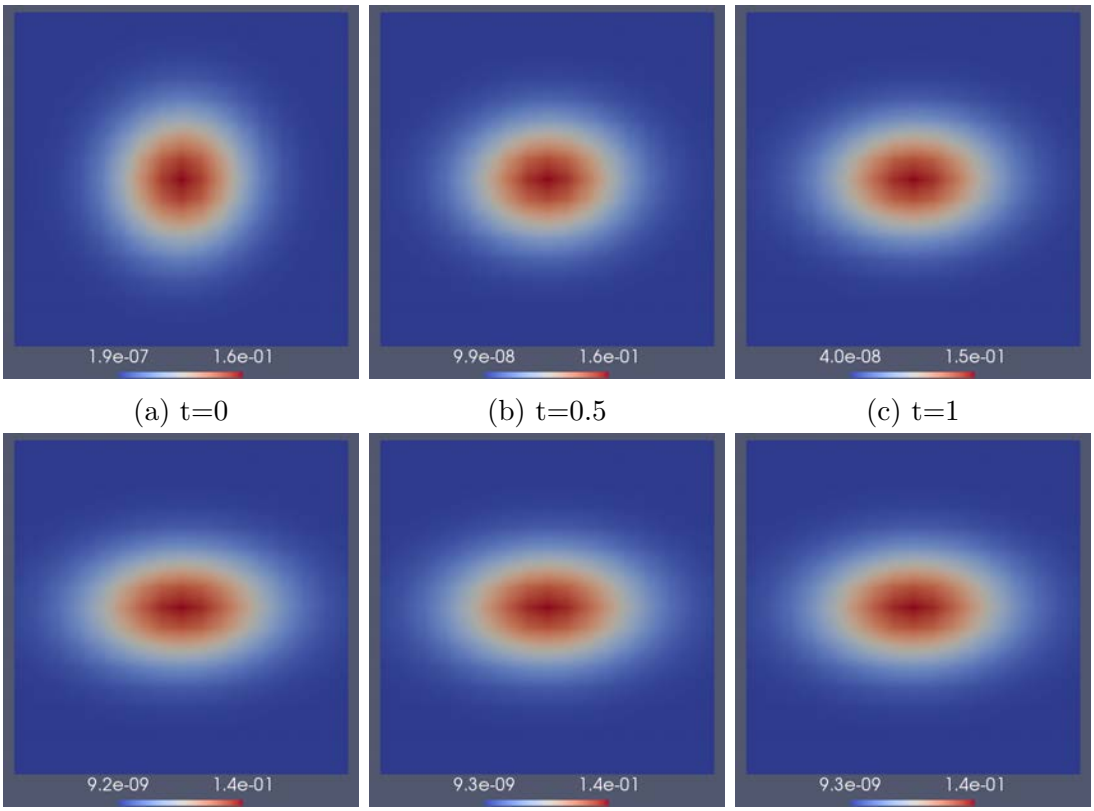

(a) t=0 (b) t=0.5 (c) t=1

(d) t=2 (e) t=10 (f) steady state

Figure 3: Experiment 3: time evolution of ψ towards the steady state

Table 1: Experiment 3: numerical error

N	5	8	10	16	20	30	40
$\|e_\psi\|_{L^2(\mathfrak{D})}$	3.4e-2	2.1e-2	1.3e-2	3.3e-3	1.3e-3	1.5e-4	1.8e-5
$\|e_\psi\|_{L^\infty(\mathfrak{D})}$	1.9e-2	7.6e-3	4.8e-3	1.2e-3	5.0e-4	5.7e-5	8.0e-6

of N. We validate these results experimentally in Figure 4, in which we plot the time evolution of mass for different values of the Hermite polynomial degree N.

4 Application to viscoelastic polymeric fluids

In the present section we aim to solve the Navier-Stokes-Fokker-Planck system describing the unsteady motion of viscoelastic fluids with infinitely extensible molecular chains. To deal with such a challenging problem we propose a multiscale scheme as a combination of the scheme (19) for the high-dimensional Fokker-Planck equation with a stabilized Lagrange-Galerkin method for the Navier-Stokes equations.

Let us mention that for a multiscale simulation of some kinetic viscoelastic models confined to bounded domains, both in the physical and the configuration

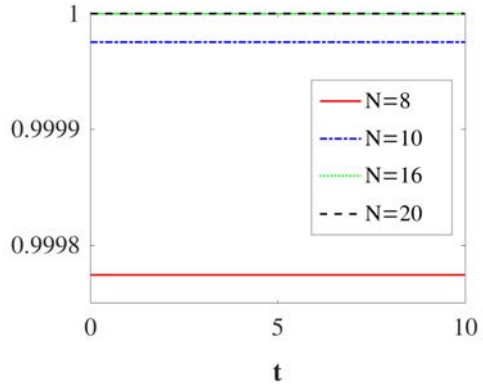

Figure 4: Evolution of mass $\int_{\mathfrak{D}} \psi_{h,N}\, d\mathbf{R}$

space, we can already find several results in the literature; for instance, [1,7,15,18] for the most commonly studied FENE model (finitely extensible nonlinear elastic); [14] for the Doi model with rod-like molecules of finite length. However, the methods developed for bounded domains can not, in general, be efficiently extended to the case of the infinite configuration space. To the best of our knowledge there are no available multiscale simulation methods for polymer solutions with infinitely extensible molecules.

4.1 The Navier-Stokes-Fokker-Planck system

We are interested in the following system of equations

$$\frac{\partial \mathbf{u}}{\partial t} + \mathbf{u}\cdot\nabla\mathbf{u} = -\nabla p + 2\nu\nabla\cdot\mathbf{D}(\mathbf{u}) + \nabla\cdot\mathbf{T}, \quad \nabla\cdot\mathbf{u} = 0, \tag{21a}$$

$$\frac{\partial \psi}{\partial t} + \mathbf{u}\cdot\nabla_x\psi - \varepsilon\Delta_x\psi = -\nabla_R\cdot\big(\nabla_x\mathbf{u}\cdot\mathbf{R}\psi\big) + \nabla_R\cdot\big(\xi\mathbf{R}\psi\big) + \chi\Delta_R\psi. \tag{21b}$$

Here the couple $(\mathbf{u}, p)$ denotes the velocity and pressure, the symmetric part of the velocity gradient is given by $\mathbf{D}(\mathbf{u}) := (\nabla\mathbf{u} + (\nabla\mathbf{u})^T)/2$, and ν stands for the solvent viscosity. Each polymer molecule is represented by its orientation vector $\mathbf{R}$ that belongs to the configuration space $\mathfrak{D}$. Function ψ gives the probability of a dumbbell that it stays between $\mathbf{R}$ and $(\mathbf{R} + d\mathbf{R})$ in space $\mathfrak{D}$, at a physical point $\mathbf{x} \in \Omega$ and time $t \in [0, T]$. The system is equipped with the decay/boundary and initial conditions,

$$\psi|_{|\mathbf{R}|\to\infty} = 0, \quad \frac{\partial\psi}{\partial\mathbf{n}}|_{\partial\Omega} = \mathbf{0}, \qquad \mathbf{u}|_{\partial\Omega} = \mathbf{0}, \tag{21c}$$

$$\psi(0) = \psi^0, \qquad \mathbf{u}(0) = \mathbf{u}^0, \tag{21d}$$

where $\mathbf{u}_0$ and ψ_0 are suitable initial values. The elastic stress tensor $\mathbf{T}$ is appearing in (21a) as a forcing term on the right-hand side of the momentum equation due to the random movement of polymer molecules. It is obtained by means of Kramer's

expression,

$$\mathbf{T} = \gamma \int_{\mathfrak{D}} (\mathbf{R} \otimes \mathbf{R})\, \psi(t, \mathbf{x}, \mathbf{R})\, d\mathbf{R} - \mathbf{I}, \tag{21e}$$

where γ is a given function defined in $[0, T] \times \Omega$.

Note the above introduced Navier-Stokes-Fokker-Planck system covers a large class of models including the so-called Hookean model, whose macroscopic closure has been rigorously proved to be the well-known Oldroyd-B model, see [3]. However, we would like to emphasize that, in general, there is no *rigorous* macroscopic closure of (21b) for non-constant functions χ, ξ, γ.

4.2 Multiscale scheme

In this part we formulate a multiscale scheme for the numerical solution of the Navier-Stoke-Fokker-Planck system (21) for dilute solutions with infinitely extensible polymer molecules.

The Navier-Stokes solver We apply the Lagrange-Galerkin method described in Subsection 2.2 to the Navier-Stokes equations (21a). We define the following finite element spaces

$$V_h := X_h^2 \cap V, \;\; Q_h := X_h^1 \cap Q,$$

where $V := H_0^1(\Omega)^2$, $Q := L_0^2(\Omega)$ are the classical functions spaces, and $\mathcal{P}^1(K)$ is the polynomial space of linear functions on element K. It is well-known that the $\mathcal{P}^1/\mathcal{P}^1$-approximation of the couple $(\mathbf{u}, p)$ solving (21a) does not satisfy the inf-sup condition. Therefore we employ the Brezzi-Pitkaränta pressure stabilization [5] to obtain

$$\begin{aligned}\left(\frac{\mathbf{u}_h^n - \mathbf{u}_h^{n-1} \circ X_1(\mathbf{u}_h^{n-1}, \Delta t)}{\Delta t}, \mathbf{v}_h\right) + 2\nu\,(\mathbf{D}(\mathbf{u}_h^n), \mathbf{D}(\mathbf{v}_h)) - (p_h^n, \nabla_x \cdot \mathbf{v}_h) \\ + (\nabla_x \cdot \mathbf{u}_h^n, q_h) + \mathcal{S}_h(p_h^n, q_h) = (\mathbf{T}_h^n, \nabla_x \mathbf{v}_h)\,, \quad \text{for any } (\mathbf{v}_h, q_h) \in V_h \times Q_h, \end{aligned} \tag{22}$$

where the pressure stabilization term is given by

$$\mathcal{S}_h(p_h, q_h) := \delta_0 \sum_K h_K^2 \nabla p_h \nabla q_h, \quad \delta_0 > 0.$$

The constant δ_0 is set to 0.05 in all subsequent numerical tests.

We now propose a multiscale scheme as a coupling of two solvers: (22) for the macroscopic solvent and (19) for the high-dimensional molecular part.

Definition 3. (Multiscale scheme for the Navier-Stokes-Fokker-Planck system) *Assuming* $X_1(\mathbf{u}_h^{n-1}, \Delta t)(\Omega) = \Omega$ *we seek a solution* $\{\mathbf{u}_h^n, p_h^n, \phi_{zk}^n\}_{n=1}^{N_T} \subset V_h \times Q_h \times W_h$

satisfying

$$\frac{\phi^*_{zk}(\mathbf{x}_i) - \phi^{n-1}_{zk}(\mathbf{x}_i)}{\Delta t} = \mathbb{L}(\phi^*_{zk}(\mathbf{x}_i)) \quad \text{for } z,k = 0,\dots,N \text{ and a fixed } \mathbf{x}_i \in \mathcal{V}_h, \tag{23a}$$

$$\left(\frac{\phi^n_{zk} - \phi^*_{zk} \circ X_1(\mathbf{u}^{n-1}_h, \Delta t)}{\Delta t}, \varphi_h\right) + \varepsilon(\nabla_x \phi^n_{zk}, \nabla_x \varphi_h) = 0 \quad \text{in } \Omega \text{ for fixed } z,k, \tag{23b}$$

$$\left(\frac{\mathbf{u}^n_h - \mathbf{u}^{n-1}_h \circ X_1(\mathbf{u}^{n-1}_h, \Delta t)}{\Delta t}, \mathbf{v}_h\right) + 2\nu\left(\mathbf{D}(\mathbf{u}^n_h), \mathbf{D}(\mathbf{v}_h)\right) - (p^n_h, \nabla_x \cdot \mathbf{v}_h)$$
$$+(\nabla_x \cdot \mathbf{u}^n_h, q_h) + \mathcal{S}_h(p^n_h, q_h) = (\mathbf{T}^n_h, \nabla_x \mathbf{v}_h) \quad \text{in } \Omega, \tag{23c}$$

for any test function $(\mathbf{v}_h, q_h, \varphi_h) \in V_h \times Q_h \times W_h$. *The piecewise linear continuous approximation* $\mathbf{T}^n_h$ *is obtained by the interpolation of the discrete values* $\mathbf{T}^n(\mathbf{x}_i) = \mathbf{T}(\psi^n_{h,N}(\mathbf{x}_i, \mathbf{R}_{lj}))$ *that are computed by Kramer's expression* (21e) *and the Hermite-Gauss quadrature, where the approximate solution* $\psi^n_{h,N} \in W_h \times P^2_N$ *is computed analogously as in the scheme* (19).

Remark 3. *The Lagrange-Galerkin method in our schemes* (19) *and* (23) *is based on the mapping* X_1 *that follows the particle along the characteristic curve backward in time. A question of our further study is to prove that the upwind point* $X_1(\mathbf{u}^{n-1}_h, \Delta t)(\mathbf{x})$ *remains in the domain* Ω, *analogously as in [24] for the case of no-slip boundary condition. However, we can ensure that* $X_1(\Omega) \subset \Omega$ *in all numerical experiments without imposing any condition on* Δt. *In the case of periodic boundary condition, we slightly modify the computation of the upwind point. For instance, if the flow is periodic in* x *direction, we first compute* $X_1(\mathbf{u}^{n-1}_h, \Delta t)(\mathbf{x}) := \mathbf{x} - \mathbf{u}^{n-1}_h(\mathbf{x})\Delta t$. *Next, we update the first component* $X_{1,1}(\mathbf{x})$ *of* $X_1(\mathbf{x})$ *as follows*

$$X_{1,1}(\mathbf{x}) = \begin{cases} X_{1,1}(\mathbf{x}) & \text{if } X_{1,1}(\mathbf{x}) \in [x_a, x_b], \\ X_{1,1}(\mathbf{x}) + (x_b - x_a) & \text{if } X_{1,1}(\mathbf{x}) < x_a, \\ X_{1,1}(\mathbf{x}) - (x_b - x_a) & \text{if } X_{1,1}(\mathbf{x}) > x_b, \end{cases}$$

for any $\mathbf{x} \in \Omega = [x_a, x_b] \times [y_a, y_b]$.

Remark 4. *Due to same reasons as explained in Remark 2 the multiscale scheme* (23) *has no requirements on the time step* Δt.

4.3 Numerical experiments

We demonstrate the performance of the multiscale scheme (23) and confirm the conservation of mass numerically. Similarly as in Subsection 3.2, the initial value of the probability density is always $\psi^0(\mathbf{x}, \mathbf{R}) = M(\mathbf{R})$, cf. (20).

Experiment 4 We consider a *driven cavity flow* as one of the benchmark problems for viscoelastic fluids. Motivated by the Peterlin dumbbell theories for dilute polymer solutions [26] we choose functions ξ and χ to be dependent on the average length of polymer molecules that is a macroscopic quantity only, namely the trace of the conformation tensor

$$\mathbf{C} := \int_{\mathbb{R}^d} (\mathbf{R} \otimes \mathbf{R}) \psi(t, \mathbf{x}, \mathbf{R}) \, d\mathbf{R}, \tag{24}$$

which is a symmetric positive definite tensor characterizing the elastic property of polymer solutions. In particular, we set $\xi = \chi = (\mathrm{tr}\mathbf{C})^2$. Further, $\gamma = 1$, $\varepsilon = 0$, $\nu = 0.59$ and $\Delta t = 0.05$. The boundary condition for the velocity is set as $\mathbf{u} = (16x_1^2(1-x_1)^2, 0)^T$ on the top boundary of the physical domain $\Omega = [0,1]^2$ and zero otherwise. Figure 5 depicts the contour lines of pressure, the values of the velocity and the conformation tensor at $t = 2$.

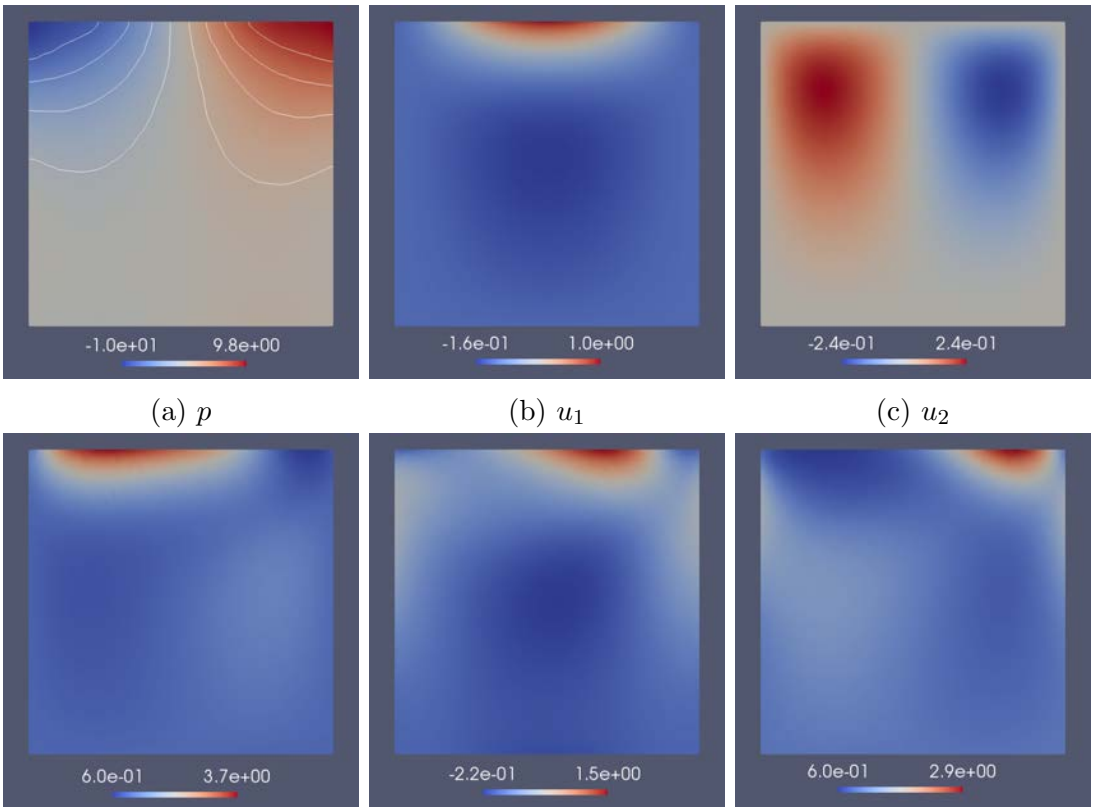

(a) p (b) u_1 (c) u_2

(d) C_{11} (e) C_{12} (f) C_{22}

Figure 5: Experiment 4: solution at time $t = 2$

Experiment 5 We now test a periodic plane *Poiseulle flow* in computational domain $\Omega = [0,1]^2$. The initial value for the velocity is $\mathbf{u}^0(\mathbf{x}) = \big(x_2(1-x_2), 0\big)^T$. In the horizontal direction we set the periodic boundary conditions for $\mathbf{u}$ and ψ. The upper and bottom boundaries are treated as no-slip walls with respect to the

velocity. In addition, the homogeneous Neumann boundary condition is adopted for ψ on the latter boundaries. We set $\Delta t = h$, the model parameters $\nu = 0.5$, $\varepsilon = 0$, and $\chi = \xi = \gamma = 1$. This choice covers the well-known Hookean model and thus allows us to find the explicit form of the conformation tensor from its macroscopic closure (Oldroyd-B model), i.e.,

$$C_{11} = 1 + \frac{1}{2}\left|\frac{\partial u_1}{\partial x_2}\right|^2 \left(1 - (2t+1)e^{-2t}\right), \quad C_{12} = \frac{1}{2}\frac{\partial u_1}{\partial x_2}(1 - e^{-2t}), \quad C_{22} = 1, \quad (25)$$

see [29, Chapter 4.1] for more details. Figure 6 shows that the numerical solution matches the analytical values (25), see the relative errors $\|e_v\| := \frac{\|v - v_{ref}\|}{\|v_{ref}\|}$ for $v \in \{\mathbf{u}, C_{11}, C_{12}, C_{22}\}$ in Table 2. Moreover, the table also indicates the numerical error is decreasing with decreasing mesh size h and increasing Hermite polynomial degree N.

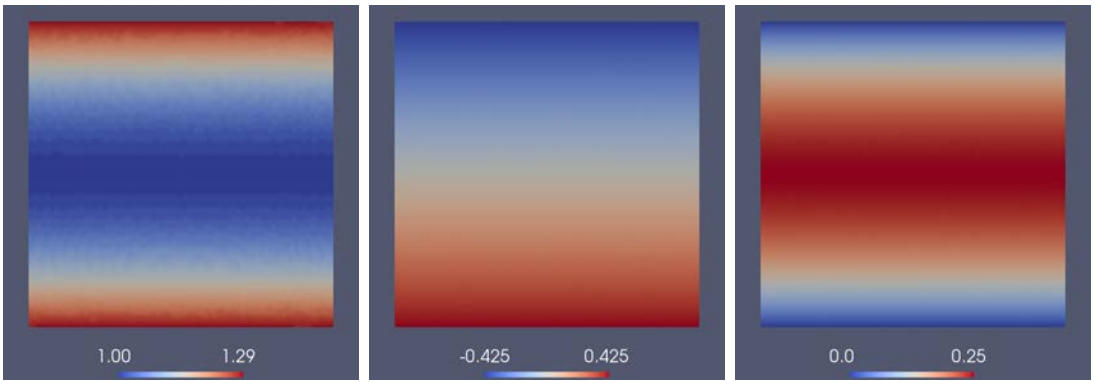

(a) C_{11} (b) C_{12} (c) u_1

Figure 6: Experiment 5: solution at time $t = 1$

Table 2: Experiment 5: numerical error at $t = 1$

$1/h$	N	$\|e_{\mathbf{u}}\|_{L^2(\Omega)}$	$\|e_{\mathbf{u}}\|_{H^1(\Omega)}$	$\|e_{C_{11}}\|_{L^2(\Omega)}$	$\|e_{C_{12}}\|_{L^2(\Omega)}$	$\|e_{C_{22}}\|_{L^2(\Omega)}$
16	8	2.15e-3	1.11e-2	3.17e-2	6.41e-2	2.82e-2
32	12	5.17e-4	4.33e-3	5.30e-3	1.45e-2	2.64e-3
64	16	1.30e-4	2.24e-3	2.58e-3	7.85e-3	1.53e-3

Experiment 6 Here we present the performance of the multiscale solver for *flow past cylinder* test, a widely studied benchmark problem with complex geometry. We set $\gamma = 1$, $\chi = \mathrm{tr}\mathbf{C}$ and $\xi = (\mathrm{tr}\mathbf{C})^2$. The boundary conditions are the same as in Experiment 5 and the inlet velocity reads $\mathbf{u} = \left(\frac{1}{4}x_2(1 - x_2), 0\right)^T$. See Figure 7 for the numerical solution for $T = 4$, $\Delta t = 0.01, \nu = 0.59$, $\varepsilon = 1$.

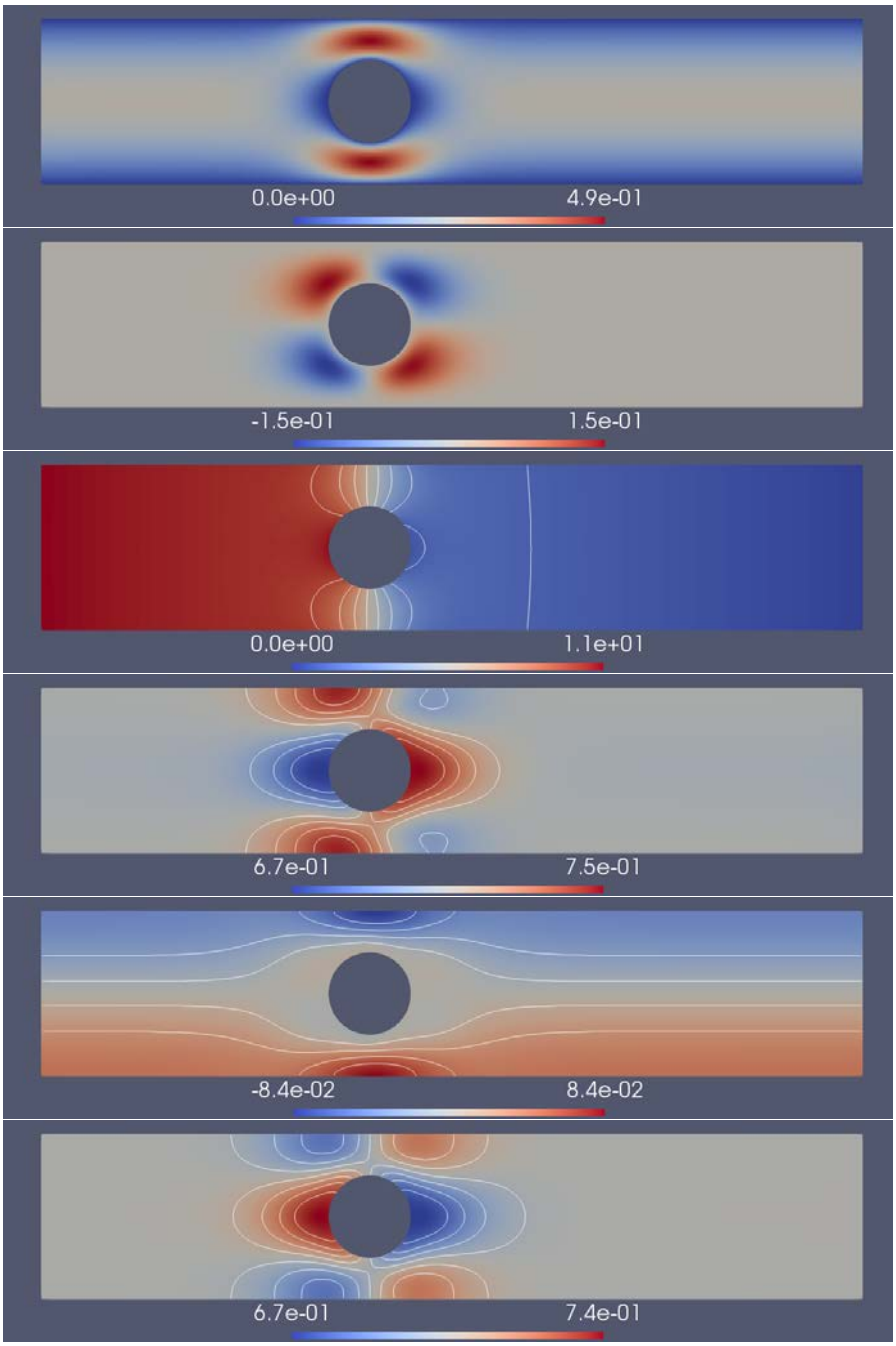

Figure 7: Experiment 6: solution of u_1, u_2, p, C_{11}, C_{12}, C_{22} (from top to bottom)

Conservation of mass Analogously as in Section 3.2, in Figure 8 we plot the time evolution of the discrete mass to validate the theoretical results numerically.

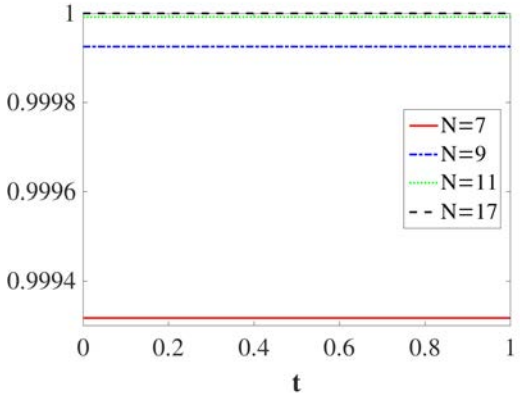

Figure 8: Evolution of mass $\int_{\mathfrak{D}} \psi_{h,N}\, d\mathbf{R}$

Conclusion

Inspired by the models of some viscoelastic polymeric fluids with infinitely extensible molecules we have studied a Navier-Stokes-Fokker-Planck system numerically. Firstly, in Definition 2, we have proposed the conservative scheme for numerical solution of the high-dimensional Fokker-Planck equation by splitting it into two parts: the first part in the bounded physical space was solved by the Lagrange-Galerkin method, while the second part in the infinite configuration space was approximated by the Hermite spectral method. Further, combining our scheme with a stabilized Lagrange-Galerkin method we derived the multiscale scheme for numerical solution of the full Navier-Stokes-Fokker-Planck system, see Definition 3.

To demonstrate the performance of our solver, we have presented several numerical experiments, from which we could conclude the numerical convergence for decreasing physical mesh size h and increasing number of grid points in the configuration space N (degree of the Hermite polynomial) as well, see Subsections 3.2 and 4.3. Moreover, in Theorem 3.1 we have theoretically proven that the discrete mass with respect to the probability density is preserved which has also been confirmed by the numerical tests. Note that for better readability we have defined the schemes only in two space dimensions, however they can be straightforwardly extended to the three-dimensional case with $\Omega \subset \mathbb{R}^3$ and $\mathfrak{D} = \mathbb{R}^3$.

To the best of our knowledge, this is the first result on the numerical simulation of the Navier-Stokes-Fokker-Planck system of equations confined to the finite physical space and the infinite configuration space.

Acknowledgements

The authors would like to thank Prof. Dr. M. Lukáčová-Medvid'ová (University of Mainz) for the fruitful discussions on this topic and Dr. K. Werth (University of Mainz) for his help with the code optimization.

References

[1] A. Abedijaberi and B. Khomami, *Continuum and multi-scale simulation of mixed kinematics polymeric flows with stagnation points: closure approximation and the high Weissenberg number problem*, J. Non-Newton. Fluid Mech., 166 (2011), pp. 533–545.

[2] J.W. Barrett and E. Süli, *Existence and equilibration of global weak solutions to kinetic models for dilute polymers I: finitely extensible nonlinear bead-spring chains*, Math. Models Methods Appl. Sci., 21 (2011), pp. 1211–1289.

[3] J.W. Barrett and E. Süli, *Existence of global weak solutions to the kinetic Hookean dumbbell model for incompressible dilute polymeric fluids*, Nonlinear Anal.-Real., 39 (2018), pp. 362–395.

[4] Barrett, J.W. and Süli, E., *Existence of global weak solutions to compressible isentropic finitely extensible nonlinear bead-spring chain models for dilute polymers: the two-dimensional case*, J. Differ. Equations, 261 (2016), pp. 592–626.

[5] F. Brezzi and J. Pitkäranta, *On the stabilization of finite element approximations of the Stokes equations*, in Efficient Solutions of Elliptic Systems, W Hackbusch, ed., Vieweg, Wiesbaden, 1984, pp. 11–19.

[6] C. Le Bris and T. Lelièvre, *Micro-macro models for viscoelastic fluids: modelling, mathematics and numerics*, Sci. China Math., 55 (2012), pp. 353–384.

[7] C. Chauvière and A. Lozinski, *Simulation of dilute polymer solutions using a Fokker–Planck equation*, Comput. Fluids, 33 (2004), pp. 687–696.

[8] P.G. Ciarlet, *The Finite Element Method for Elliptic Problems*, Studies in Mathematics and its Applications, Elsevier Science, 1978.

[9] M. Doi and S.F. Edwards, *The Theory of Polymer Dynamics*, International series of monographs on physics, Clarendon Press, 1988.

[10] J. Douglas Jr and T. F. Russell, *Numerical methods for convection-dominated diffusion problems based on combining the method of characteristics with finite element or finite difference procedures*, SIAM J. Numer. Anal., 19 (1982), pp. 871–885.

[11] J.C.M. Fok, B. Guo, and T. Tang, *Combined Hermite spectral-finite difference method for the Fokker-Planck equation*, Math. Comput., 71 (2002), pp. 1497–1528.

[12] T.D. Frank, *Nonlinear Fokker-Planck Equations: Fundamentals and Applications*, Springer Series in Synergetics, Springer Berlin Heidelberg, 2005.

[13] Gwiazda, P. and Lukáčová-Medviďová, M. and H. Mizerová and Świerczewska-Gwiazda, A., *Existence of global weak solutions to the kinetic Peterlin model*, Nonlinear Anal.-Real, 44 (2018), pp. 465–478.

[14] C. Helzel and F. Otto, *Multiscale simulations for suspensions of rod-like molecules*, J. Comput. Phys., 216 (2006), pp. 52–75.

[15] D.J. Knezevic and E. Süli, *A heterogeneous alternating-direction method for a micro-macro dilute polymeric fluid model*, ESAIM: M2AN, 43 (2009), pp. 1117–1156.

[16] D.J. Knezevic and E. Süli, *Spectral Galerkin approximation of Fokker-Planck equations with unbounded drift*, ESAIM: M2AN, 43 (2009), pp. 445–485.

[17] P. D. Lax and A. N. Milgram, *Parabolic Equations*, in Contributions to the Theory of Partial Differential Equations, Lipman Bers, Salomon Bochner, and Fritz John, eds., vol. 33 of Annals of Mathematics, Princeton University Press, Berlin, Boston, 1955, ch. IX.

[18] A. Lozinski and C. Chauvière, *A fast solver for Fokker-Planck equation applied to viscoelastic flows calculations: 2D FENE model*, J. Comput. Phys., 189 (2003), pp. 607–625.

[19] M. Lukáčová-Medviďová, H. Mizerová, H. Notsu, and M. Tabata, *Numerical analysis of the Oseen-type Peterlin viscoelastic model by the stabilized Lagrange–Galerkin method, Part I: A nonlinear scheme*, ESAIM: M2AN, 51 (2017), pp. 1637–1661.

[20] M. Lukáčová-Medviďová, H. Mizerová, H. Notsu, and M. Tabata, *Numerical analysis of the Oseen-type Peterlin viscoelastic model by the stabilized Lagrange–Galerkin method, Part II: A linear scheme*, ESAIM: M2AN, 51 (2017), pp. 1663–1689.

[21] M. Lukáčová-Medviďová, H. Notsu, and B. She, *Energy dissipative characteristic schemes for the diffusive Oldroyd-B viscoelastic fluid*, Int. J. Numer. Methods Fluids, 81 (2016), pp. 523–557.

[22] M. Mohammadi and A. Borzi, *A Hermite spectral method for a Fokker-Planck optimal control problem in an unbounded domain*, Int. J. Uncertain. Quantif., 5 (2015), pp. 233–254.

[23] H. Notsu and M. Tabata, *Error estimates of a pressure-stabilized characteristics finite element scheme for the Oseen equations*, J. Sci. Comput., 65 (2015).

[24] H. Notsu and M. Tabata, *Error estimates of a stabilized Lagrange-Galerkin scheme for the Navier-Stokes equations.*, ESAIM: M2AN, 50 (2016), pp. 361–380.

[25] O. Pironneau and M. Tabata, *Stability and convergence of a Galerkin-characteristics finite element scheme of lumped mass type*, Int. J. Numer. Methods Fluids, 64, pp. 1240–1253.

[26] M. Renardy, *Mathematical Analysis of Viscoelastic Flows*, CBMS-NSF Regional Conference Series in Applied Mathematics, Society for Industrial and Applied Mathematics, 2000.

[27] H. Risken, *The Fokker-Planck Equation: Methods of Solution and Applications*, Springer Series in Synergetics, Springer Berlin Heidelberg, 2012.

[28] H. Rui and M. Tabata, *A second order characteristic finite element scheme for convection-diffusion problems*, Numer. Math., 92 (2002), pp. 161–177.

[29] B. She, *Numerical simulation of some viscoelastic fluids*, PhD thesis, University of Mainz, Germany, 2015.

[30] J. Shen, T. Tang, and L. Wang, *Spectral methods. Algorithms, analysis and applications.*, Berlin: Springer, 2011.

[31] J. Shen and L. Wang, *Some recent advances on spectral methods for unbounded domains*, Commun. Comput. Phys., 5 (2009), pp. 195–241.

[32] J. Shen and H. Yu, *On the approximation of the Fokker-Planck equation of the finitely extensible nonlinear elastic dumbbell model I: A new weighted formulation and an optimal spectral-Galerkin algorithm in two dimensions*, SIAM J. Numer. Anal., 50 (2012), pp. 1136–1161.

[33] E. Süli, *Convergence and nonlinear stability of the Lagrange-Galerkin method for the Navier-Stokes equations*, Numer. Math., 53 (1988), pp. 459–483.

[34] T. Tang, S. McKee, and M.W. Reeks, *A spectral method for the numerical solutions of a kinetic equation describing the dispersion of small particles in a turbulent flow*, J. Comp. Phys., 103 (1992), pp. 222 – 230.